Development of high-performance graphene-HgCdTe detector technology for mid-wave infrared applications

Sood, Ashok, Zeller, John, Ghuman, Parminder, Babu, Sachidananda, Dhar, Nibir, et al.

Ashok K. Sood, John W. Zeller, Parminder Ghuman, Sachidananda Babu, Nibir K. Dhar, Samiran Ganguly, Avik W. Ghosh, "Development of high-performance graphene-HgCdTe detector technology for mid-wave infrared applications," Proc. SPIE 11129, Infrared Sensors, Devices, and Applications IX, 1112906 (9 September 2019); doi: 10.1117/12.2531651

SPIE.

Event: SPIE Optical Engineering + Applications, 2019, San Diego, California, United States

Development of High-Performance Graphene-HgCdTe Detector Technology for Mid-wave Infrared Applications

Ashok K. Sood and John W. Zeller
Magnolia Optical Technologies, 52-B Cummings Park, Suite 314, Woburn, MA 01801

Parminder Ghuman and Sachidananda Babu
NASA Earth Science Technology Office, Greenbelt, MD 20771

Nibir K. Dhar
U.S. Army C5ISR Center Night Vision & Electronic Sensors Directorate
Fort Belvoir, VA 22060

Samiran Ganguly and Avik W. Ghosh
Department of Electrical & Computer Engineering, University of Virginia,
Charlottesville, VA 22904

ABSTRACT

A high-performance graphene-based HgCdTe detector technology is being developed for sensing over the mid-wave infrared (MWIR) band for NASA Earth Science, defense, and commercial applications. This technology involves the integration of graphene into HgCdTe photodetectors that combines the best of both materials and allows for higher MWIR (2-5 μm) detection performance compared to photodetectors using only HgCdTe material. The interfacial barrier between the HgCdTe-based absorber and the graphene layer reduces recombination of photogenerated carriers in the detector. The graphene layer also acts as high mobility channel that whisks away carriers before they recombine, further enhancing the detector performance. Likewise, HgCdTe has shown promise for the development of MWIR detectors with improvements in carrier mobility and lifetime. The room temperature operational capability of HgCdTe-based detectors and arrays can help minimize size, weight, power and cost for MWIR sensing applications such as remote sensing and earth observation, e.g., in smaller satellite platforms. The objective of this work is to demonstrate graphene-based HgCdTe room temperature MWIR detectors and arrays through modeling, material development, and device optimization. The primary driver for this technology development is the enablement of a scalable, low cost, low power, and small footprint infrared technology component that offers high performance, while opening doors for new earth observation measurement capabilities.

Keywords: Graphene, HgCdTe, MCT, photodetectors, MWIR, mobility, lifetime, high operating temperature

1. INTRODUCTION

Infrared detector and focal plane array (FPA) technologies are at the heart of many remote sensing instruments for a multitude of NASA and defense missions. Detection of mid-wave infrared (MWIR) radiation benefits applications including long-range imaging and early threat detection [1]. It is also useful for measuring natural features including sea surface temperature, cloud properties, volcanic activities, and forest fires. The 2-5 μm MWIR spectral band is likewise suitable for a variety of NASA Earth Science applications. Using low size, weight, power, and cost MWIR sensors on smaller platforms in space can offer improved measurement and mission capabilities.

Cryogenic cooling is often utilized to minimize thermally generated dark current, and since dark current increases with longer cutoff wavelengths the requirement for cooling becomes even more important for longer wavelength MWIR and long-wave infrared (LWIR) sensors. Therefore, it is very desirable to develop infrared detector technologies that operate at or near room temperature, thus avoiding costly and bulky cooling requirements.

HgCdTe is the most widely used infrared (IR) detector material in military applications due primarily to its properties as a direct energy bandgap semiconductor and the tunability of its bandgap by varying the Cd composition to cover a broad

Infrared Sensors, Devices, and Applications IX, edited by Paul D. LeVan, Priyalal Wijewarnasuriya, Ashok K. Sood, Proc. of SPIE Vol. 11129, 1112906
 · doi: 10.1117/12.2531651

range of wavelengths from near-infrared (NIR) to very long wavelength infrared (VLWIR) [2]. Typically, an 0.3:0.7 Cd:Hg ratio results in a detectivity window in the short-wave infrared (SWIR) to MWIR range Additionally, HgCdTe layer growth can be highly controlled using techniques such as molecular beam epitaxy (MBE), which yields high precision in the deposition of detector material structures leading to excellent control over optical excitation. This is evidenced by the high quantum efficiencies (QE) demonstrated by HgCdTe for infrared detection.

The incorporation of a high mobility graphene channel serves to further enhance the HgCdTe-based detector performance and operational capabilities. The intrinsic interfacial barrier between the HgCdTe-based absorber and the graphene layer can effectively reduce recombination of photogenerated carriers in the detector. The graphene functions as a high mobility channel that whisks away carriers before they can recombine, further contributing to the MWIR performance of graphene-integrated HgCdTe photodetectors compared to that of HgCdTe-only detectors.

For the MBE material growth and processing of the graphene-enhanced MWIR photodetectors and FPAs, we are collaborating with the U.S. Army Night Vision and Electronic Sensors Directorate (NVESD), as well as capitalizing on facilities available to us at Albany Nanotech, also known as the College of Nanoscale Science and Engineering (CNSE), SUNY Polytechnic Institute (SUNY Poly) in Albany, NY. Figure 1 gives an overview of the SUNY Poly CNSE campus.

Figure 1. Albany Nanotech (SUNY Poly) campus in Albany, NY. Magnolia Optical Technologies office is collocated in the SUNY Poly complex and has access to wafer processing facilities.

2. HGCDTE-GRAPHENE DETECTOR ARCHITECTURE AND OPERATION

2.1 HgCdTe-graphene detector architecture

A schematic of the proposed detector structure is shown in Figure 2. The detector, which comprises three principal layers, is grown over a silicon substrate with a layer of CdTe grown on it acting as a buffer. The Si substrate layer functions as the gate terminal, which provides an electrical field in the "vertical" direction into the detector heterostructure. This field aids in carrier transport in the vertical direction.

The absorber layer, grown on top of the silicon substrate and CdTe buffer layer, acts as the active optical layer where photogeneration of carriers takes place. The absorber material and its physical properties, such as the bandgap between conduction and valence bands, determine the absorber layer's sensitivity to the detection wavelength window. In addition, the absorber material also determines the photogeneration rate, quantum efficiency, and carrier lifetime, which collectively govern the overall detector performance.

The graphene layer occupies the role of a high mobility, low noise channel that can quickly whisk the photogenerated carriers in the absorber away into the contacts, and subsequently into the readout integrated circuit (ROIC) for electrical readout. Therefore, this layer is directly contacted to the ROIC.

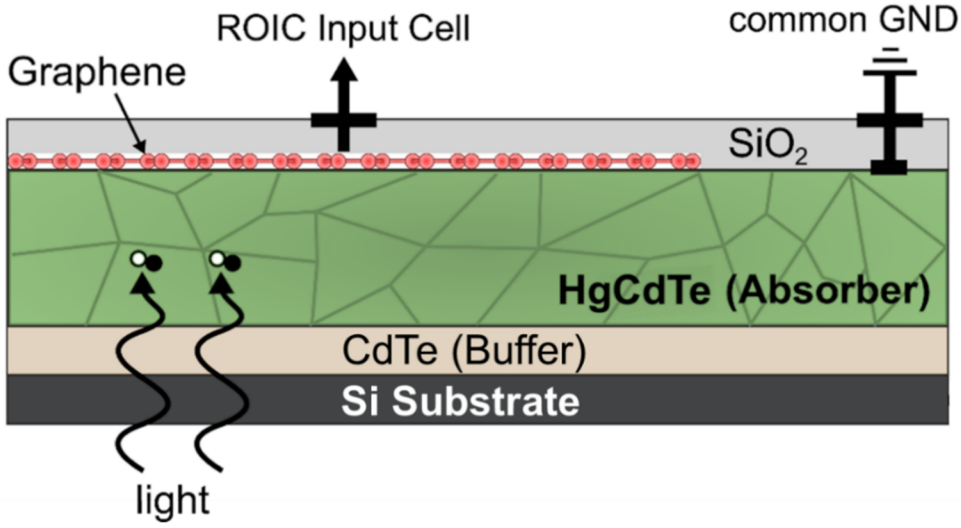

Figure 2. Polycrystalline HgCdTe-graphene heterostructure based IR photodetector structure.

2.2 Detector operating principle

The general operating principle of the graphene-HgCdTe photodetector can be described in terms of the life cycle of the photogenerated carriers. Incident IR photons are transmitted through the Si substrate and CdTe layers into the absorber region, where they are absorbed to produce electron-hole pairs, or excitons (Figure 3). The vertical electrical field in the absorber applied through modulation of the gate electric field separates the electron-hole pairs due to the opposing forces on the electrons and holes that dominate the internal electron hole pair electrostatic attraction. This separation of the carriers is critical to the performance of the detector as it physically isolates the two photogenerated carrier species and suppresses the Auger recombination within the absorber, thus minimizing the loss of photogenerated carriers.

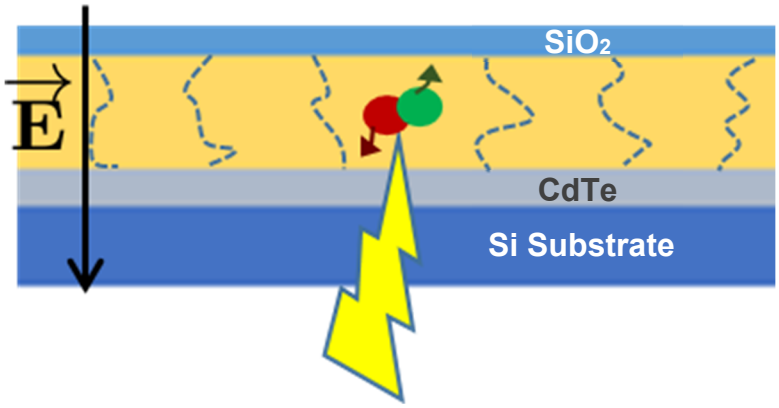

Figure 3. Generation of excitons due to incident photons and separation into electrons and holes due to gate electric field.

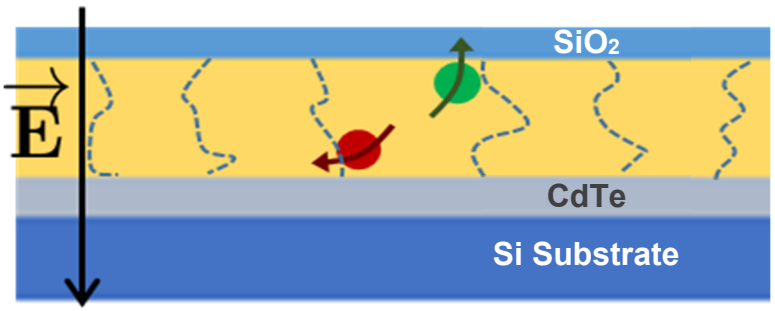

Figure 4. Photogenerated carrier transport and injection into graphene.

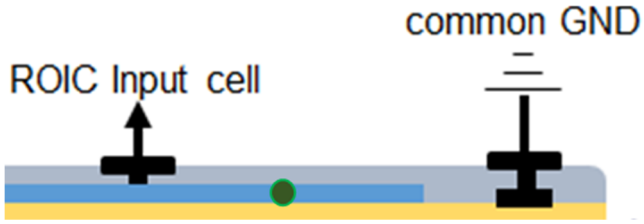

Figure 5. Horizontal transport of photogenerated carriers in graphene.

After separation, the carriers are transported through the absorber film towards the graphene interface and then injected into it (Figure 4). Using a detailed electrostatic model, the gate voltage bias can be utilized to dynamically control the interface properties and preferentially inject only one of the photogenerated species into the graphene, in a rectifier-like action. This further prevents any Auger recombinations in the graphene due to injection of both species. The blocked carriers may be collected away in a separate grounded terminal.

The carriers injected from the absorber into the graphene are transported in the lateral direction and delivered to the ROIC terminal and subsequently collected into it (Figure 5). Developing a separate high mobility channel like graphene allows faster modulation frequencies with reduced 1/*f* noise and consequently higher performance metrics. In addition, the electrical control of the carrier injection into the graphene allows for dynamic gating.

3. MODELING OF GRAPHENE-HGCDTE DETECTOR

3.1 Modeling approach

The overall modeling effort is built upon various individual pieces that combine to build a comprehensive model for this detector technology. The goal of the modeling effort is to generate accurate electrical behavior (such as I-V characteristics), noise, responsivity, and performance metrics (such as D^* and NEDT) from basic material parameters and device design and operating specifications, through simulations. This allows for design optimization in terms of constraints placed by design rules and fabrication capabilities.

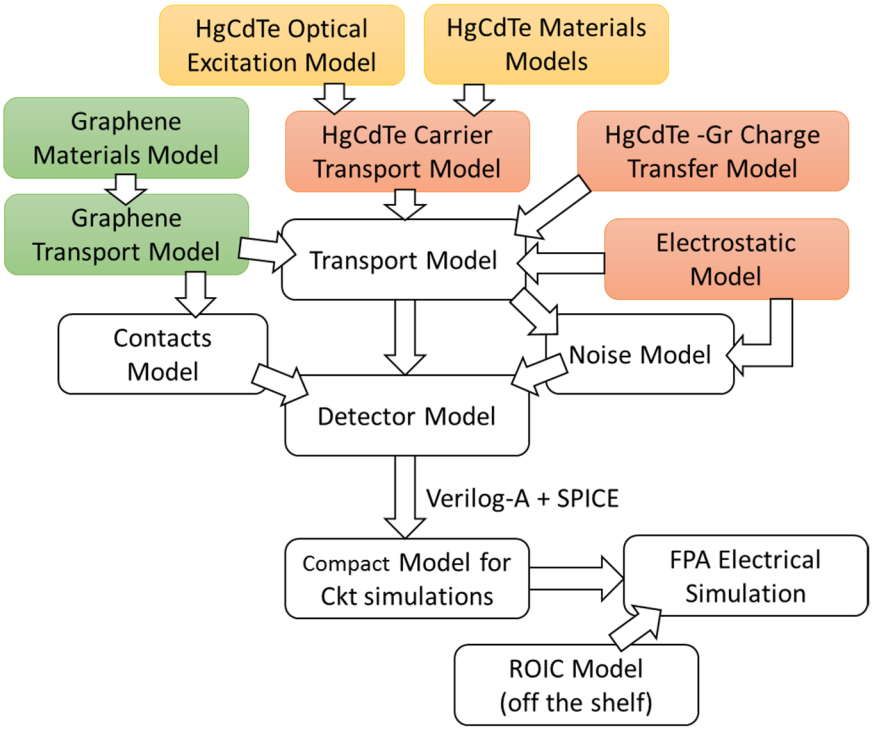

Figure 6. Flowchart schematic diagram illustrating modeling approach and relationship between utilized models.

The modeling effort is depicted schematically in Figure 6. The overall modelling plan involves modularly constructing the complete detector simulation platform from individual models as data is made available from experiments and device characterization. These including individual materials models for HgCdTe, graphene, and the HgCdTe-graphene interface, which are described in the following sections.

3.2 HgCdTe materials model

Materials modeling can refer many different things depending on the situation and application. Here a *materials model* is defined as a mathematical description of an energy dispersion relation, graphically represented as *E-k* diagrams that relate the carrier transport (momentum) to the allowed energy states in the material in view. From this model properties of interest can be related, including but not limited to current, photoexcitation, recombination velocity, lifetime, and noise.

The HgCdTe materials modeling is being approached separately from the graphene charge carrier transport modeling at present. In the future we plan to connect these two efforts by modeling HgCdTe-graphene using the charge transfer method, which requires rigorous understanding of heterostructure material interface properties. An exact electrostatic model is necessary as well to predict charge flow in this heterostructure.

3.3 Graphene materials model

Graphene is composed of a hexagonal lattice arrangement of carbon atoms. In the bonding process the *px* and *py* orbitals take part, while the *pz* orbital lies above the plane and provides sites for current conduction. Being removed from the 2-D plane of the graphene, these carriers suffer low scattering and hence can have very high mobilities, though charges accumulating at the surface due to nonuniformity of chemical and electrostatic doping levels can change this considerably.

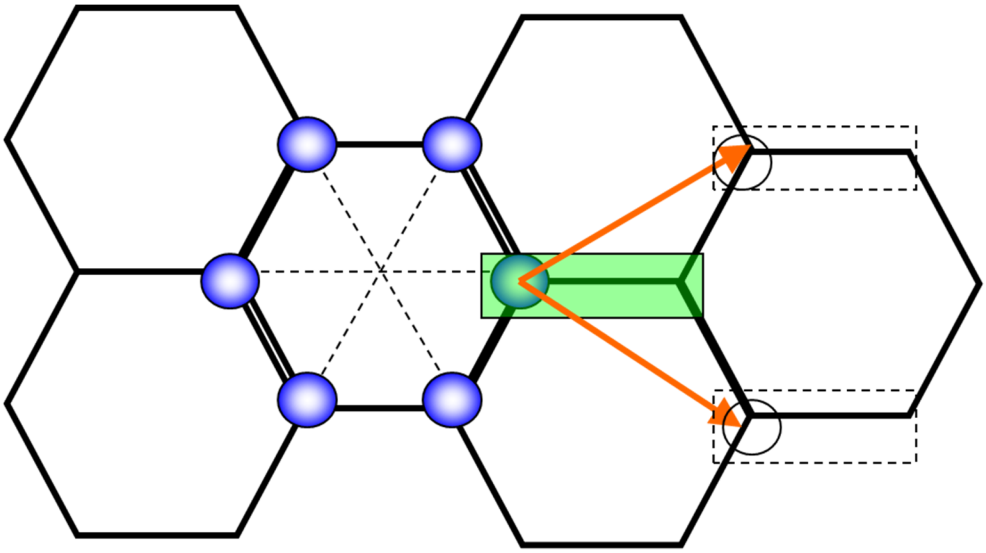

Figure 7. Schematic depiction of exact tight-binding model for graphene using a two-atom basis set. The in-plane bonds are due to hybridized *px-py* orbitals, while the *pz* orbital lobes lie outside the plane of the sheet.

An exact tight-binding model for graphene can be developed using a two-atom basis set as shown in Figure 7. Using this method, it is possible to analytically obtain the infinite extent graphene *E-k* relationship, where the bands at low biases look like cones which touch at the Dirac (zero) point. Depending on the dimensions of the pixel, possible confinement of states along squeezed dimensions can be seen, giving rise to subbands and thus energy-dependent modes of conduction. In such a case it is not possible to analytically calculate the current flow, but rather use a numerical integration built upon a quantum non-equilibrium Green's function (NEGF) Landauer model. In the case that such confinement does not exist, a semiclassical Landauer model (Boltzmann transport equation) can be implied instead, since quantum mechanics does not play a critical role in carrier transport in such situations.

3.4 Graphene-HgCdTe interface model

It is possible to build tight-binding models for both HgCdTe as well as the graphene layer. However, a critical component of the detector operation depends on the properties of the interface between these two materials.

A density functional theory (DFT) model is being developed for the HgCdTe-graphene heteromaterial interface. DFT encompasses the most fundamental approach to calculate the energy-momentum dispersion relationship. This model enables calculation of the charge transfer that can arise between the two materials, thereby providing the upper limit of charge separation. This is critical to calculating the photocurrent or signal that can be obtained from the device, as well as the lifetime of the carriers due to charge separation or collection.

3.5 Mobility and lifetime model

Mobility models for $Hg_{1-x}Cd_xTe$ are typically valid for a range of stoichiometries and temperatures. The model presented below provides a good approximation for the Cd composition x over the range of interest from 0.2 to 0.6:

$$\mu_e = \frac{9\times10^8 s}{T^{2r}} \tag{1}$$

where s and r are given by $\left(\frac{0.2}{x}\right)^{0.6}$ and $\left(\frac{0.2}{x}\right)^{7.5}$, respectively. The mobility as a function of stoichiometry and temperature is plotted in Figure 8.

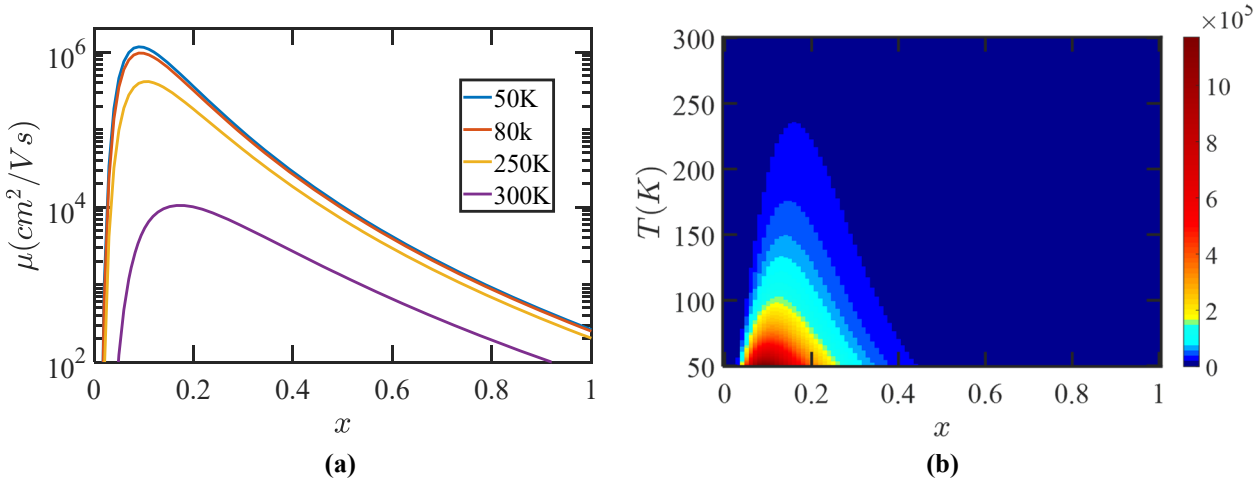

Figure 8. (a) Mobility of $Hg_{1-x}Cd_xTe$ as a function of stoichiometry at different temperatures. (b) Colormap showing the mobility over a large temperature range for different stoichiometries.

Lifetime is an important parameter in the field of IR detection. While at low temperatures the dominating factor is expected to be Shockley-Reed-Hall recombination that is mediated by trap levels in the bandgap, at higher temperatures the Auger effect is the dominating mechanism (explained by phonon statistics).

The Auger lifetime model for intrinsic HgCdTe is given using the Kinch model:

$$\tau_{Aug} = \frac{2.12x10^{-14}\sqrt{E_g}e^{\frac{qE_g}{kT}}}{FF^2\left(\frac{kT}{q}\right)^2} \tag{2}$$

There are two different kinds of Auger processes in doped HgCdTe, one driven by impact ionization of electrons (designated *Auger 1*), and the second driven by light hole impact ionization (designated *Auger 7*). *Auger 1* is given by:

$$\tau_{Auger1} = \frac{2\tau_{Auger}}{1+\left(\frac{n}{n_i}\right)^2} \tag{3}$$

where n is the doping level and n_i is the intrinsic carrier concentration. *Auger 7* typically yields a lifetime around an order of magnitude larger than *Auger 1*. The total lifetime τ_{Auger} due to the two processes is given by:

$$\tau_{Auger} = \frac{\tau_{Auger1}\tau_{Auger7}}{\tau_{Auger1}+\tau_{Auger7}} \tag{4}$$

These various lifetimes are plotted in Figure 9.

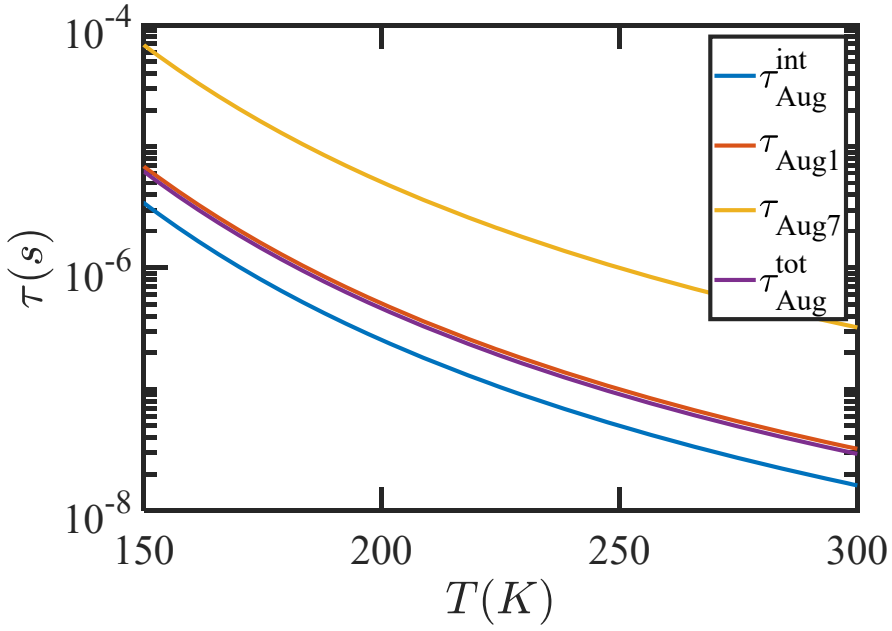

Figure 9. Various Auger lifetimes in $Hg_{1-x}Cd_xTe$ for extrinsic carrier concentration n of 1×10^{16} cm^{-3} and $x = 0.3$, as functions of temperature.

4. HGCDTE DETECTOR BANDGAP ENGINEERING AND FABRICATION

4.1 HgCdTe crystal structure and *E-k* relation

The natural zincblende or face-centered cubic (FCC) structure lattice of HgCdTe is composed of two interpenetrating sublattices of Hg or Cd (cation) with Te (anion). HgTe is a semimetal having a vanishing gap between the valence and conduction bands, while CdTe is a semiconductor with a bandgap of ~1.5 eV. Through selectively combining these two materials, it is possible to obtain a composite material with varying bandgap.

Bandgap engineering of the HgCdTe detector material is practically achieved by varying the epitaxial growth process parameters. This provides the capability to optimize the performance to achieve the spectral range and operating temperature specifications desired for the graphene-enhanced MWIR detectors and arrays. HgCdTe offers an energy bandgap that is tunable over a wide range of IR wavelengths including the 2-5 μm MWIR spectral region.

The bandgap vs. stoichiometry for $Hg_{1-x}Cd_xTe$ at various temperatures may be determined using a simple linear model:

$$E_g = xE_g^{CdTe} + (1-x)E_g^{HgTe} \tag{5}$$

However, it has been observed from experiments that due to nonidealities such as defects, this linear fit does not always provide an exact match with the actual bandgap. Therefore, the Hansen model is utilized for determining the bandgap, given by:

$$E_g(x,T) = -0.302 + 1.93x + (5.535x10^{-4})(1-2x)T - 0.81x^2 + 0.832x^3 \tag{6}$$

It is seen from Figure 9(a) that increasing the CdTe mole fraction in $Hg_{1-x}Cd_xTe$ results in wider energy bandgap and shorter cutoff wavelength. Likewise, Figure 9(b) shows a relatively slight dependence of bandgap on temperature. Thus, the stoichiometry is the most critical factor. This demonstrates that it is possible to controllably tune the absorption window of the incident light.

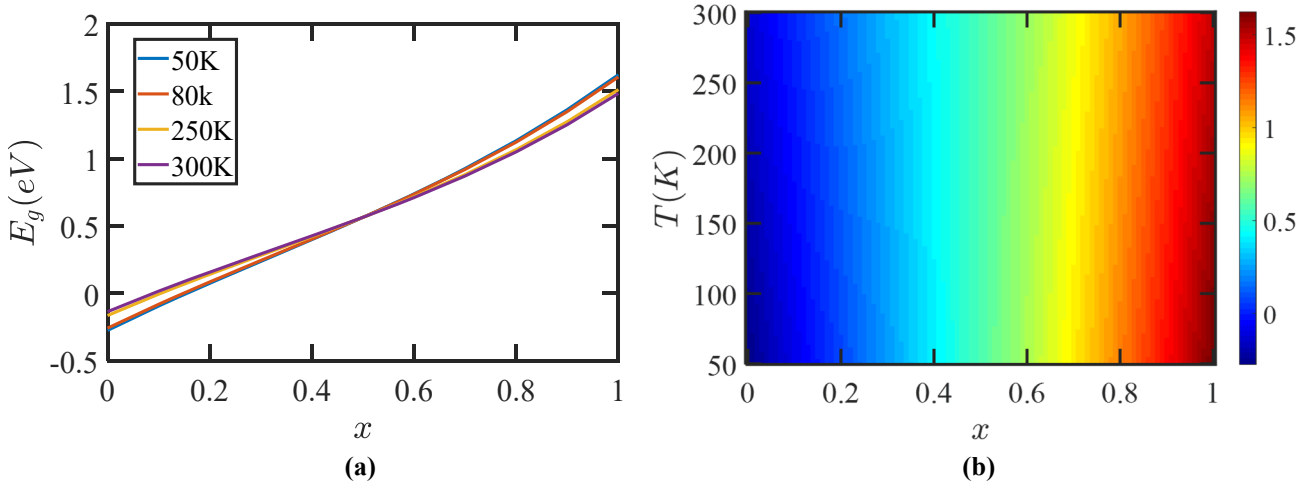

(a) (b)

Figure 10. (a) Plot of E_g vs. x for $Hg_{1-x}Cd_xTe$ at four different temperatures. Using x = 0.3 (Cd), a bandgap of 0.29 eV is obtained which corresponds to the MWIR region, whereas x = 0.4 corresponds to E_g of 0.42 eV in the SWIR range. (b) E_g plotted as a function of both T and x.

4.2 HgCdTe/CdTe/Si layer growth and band structure

Due to its relatively close lattice-matching to HgCdTe, CdZnTe has traditionally been used as the substrate material for HgCdTe-based IR detectors. However, for the device and application in view silicon substrates are desired, as they have superior surface quality with lower defect densities, are more robust and cost-effective, are available in larger sizes, and are thermally compatible with existing ROICs. The MWIR detection performance of HgCdTe epitaxially grown on Si is also comparable to that deposited on established CdZnTe wafers [1]. The capability for growing HgCdTe on larger diameter Si wafers offers the potential for low-cost, large-format graphene-enhanced FPAs with high pixel operability for detection over the 2-5 μm band.

For low size, weight, power and cost space applications, making operating temperatures as high as possible (i.e., 300 K) is desired while maintaining acceptable levels of performance. HgCdTe-based detector performance at higher operating temperatures, like that of practical photodetectors in general, is largely affected by the presence of defects and dislocations arising from lattice mismatch and resulting residual stress that shortens lifetimes and lowers the mobility of minority carriers [2]. However, the use of thermal cycle annealing processes such as postgrowth thermal cycle annealing (TCA) can produce up to an order of magnitude reduction in the dislocation density down to the saturation limit (~10^6 cm^{-2}) [3], enabling improved high temperature operability of HgCdTe-on-Si-based MWIR detectors and FPAs.

Among various silicon substrates, the Si (112) orientation is preferred for HgCdTe epitaxial growth due to Hg consumption, defect control, and doping issues [4]. The use of thinned substrates for epitaxial growth can further reduce the formation of threading dislocations towards the film surface [5]. Thinner substrates also maximize the IR radiation transmitted into the HgCdTe absorbing region, particularly benefitting backside-illuminated MWIR detectors and FPAs.

The workfunction of $Hg_{0.73}Cd_{0.27}Te$, Φ_{HgCdTe}, has been determined based on the following relation:

$$\Phi_{HgCdTe} = x\Phi_{CdTe} + (1-x)\Phi_{HgTe} \quad (7)$$

where x is the CdTe concentration in $Hg_{1-x}Cd_xTe$, and the workfunctions of CdTe and HgTe, Φ_{CdTe} and Φ_{HgTe}, are 4.5 eV and 5.9 eV, respectively [6]. As depicted in Figure 11, $Hg_{0.7}Cd_{0.3}Te$ produces a built-in voltage potential with naturally p-doped graphene of ~0.6 eV. With n-doped graphene having a workfunction 4.25, the built-in voltage would be as high as 1.27 eV. Given its intermediate workfunction between that of $Hg_{0.7}Cd_{0.3}Te$ (5.5 eV) and n-doped Si (4.1 eV), using a CdTe buffer layer thus facilitates band matching of the HgCdTe/CdTe/Si layers.

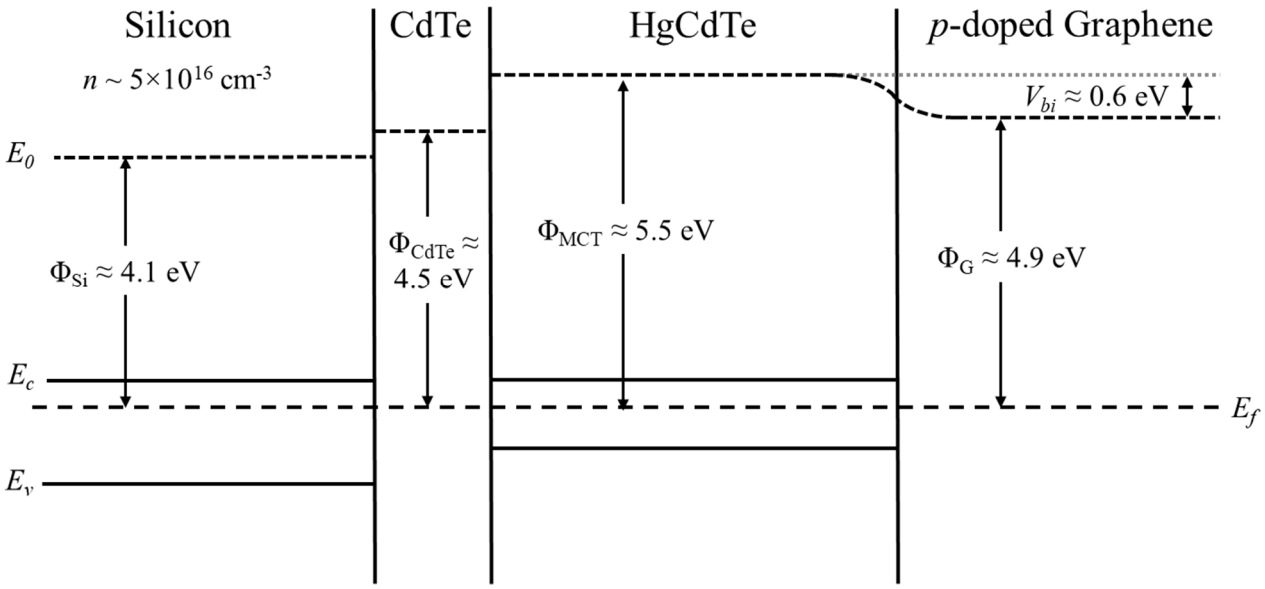

Figure 11. Band diagram for graphene/HgCdTe/Si detector heterostructure.

4.3 Graphene-HgCdTe detector fabrication technique

Molecular-beam epitaxy (MBE), a vapor phase epitaxy process, allows growth of high crystalline quality HgCdTe on Si substrates with precise control of the detector material structure parameters, where *n*-type doping of up to 1×10^{19} cm^{-3} may be achieved [1]. For MBE growth of HgCdTe on Si, use of the intermediate IR-transparent CdTe buffer layer helps reduce lattice mismatch between the HgCdTe layer and Si substrate. A process technology for fabrication of CdTe/Si(211) composite substrates by MBE has been developed by the U.S. Army Night Vision and Electronic Sensors Directorate [7]. The HgCdTe/CdTe on Si growth steps for the MWIR detector fabrication are given as follows.

Prior to the HgCdTe growth, the native oxide of the as-received Si wafers is chemically removed, leaving a hydrogen-passivated surface. The Si (211) oriented substrate is heated to temperatures high enough to desorb hydrogen [8]. The CdTe buffer layer is then deposited at ~300°C, and TCA is periodically performed throughout the growth process. Following this step, the composite CdTe-on-Si wafers are transferred to a separate MBE reactor for deposition of the HgCdTe films. The HgCdTe absorbing layer is then epitaxially grown on the buffer layer with the desired stoichiometry (e.g., $x = 0.3$) and thickness. On this layer the 2-D graphene material is grown, followed by deposition of the top metal contacts and layer of passivating oxide, to form the detector structure of Figure 1.

5. SUMMARY AND CONCLUSIONS

A high-performance graphene-HgCdTe detector technology that combines the best of both materials is being developed for MWIR sensing. The roles and functionalities of the three main MWIR detector layers have been examined, and the operating principles and electro-optical/infrared behavior of the detector described. An overview of the modeling approach, accomplished in part through development of a model for the detector band structure, has likewise been presented.

The graphene layer functions as high mobility channel that reduces recombination of photogenerated carriers in the detector. We have assessed the material and electrical properties of HgCdTe for MWIR detection and associated performance features in view of the applicational requirements, where improvements in carrier mobility and lifetime enable enhanced IR sensing performance. A fabrication process for the graphene-enhanced MWIR detectors and arrays involving MBE growth and integration of polycrystalline HgCdTe/CdTe on Si has also been discussed. The room temperature operational capability of the graphene-enhanced HgCdTe detectors and arrays can provide new earth observation measurement capabilities to benefit and advance various NASA Earth Science applications.

ACKNOWLEDGEMENTS

This research is and has been funded by the National Aeronautics and Space Administration (NASA), Contract No. 80NSSC18C0024. The views and conclusions contained in this document are those of the authors and should not be interpreted as representing the official policies, either express or implied, of NASA or the U.S. Government.

REFERENCES

[1] A. Rogalski, "HgCdTe infrared detector material: history, status and outlook," Rep. Prog. Phys. 68, 2267-2336 (2005).
[2] N. K. Dhar, R. Dat and A. K. Sood. "Advances in infrared detector array technology." In *Optoelectronics-Advanced Materials and Devices*. IntechOpen, 2013.
[3] R. N. Jacobs, J. D. Benson, A. J. Stoltz, L. A. Almeida, S. Farrell, G. Brill, M. Salmon, and A. Newell, "Analysis of thermal cycle-induced dislocation reduction in HgCdTe/CdTe/Si(211) by scanning transmission electron microscopy," J. Cryst. Growth 366, 88-94 (2013).
[4] G. Brill, Y. Chen, and P. Wijewarnasuriya, "Study of HgCdTe material grown by molecular beam epitaxy," J. Electron. Mat. 40(8), 1679-1684 (2011).
[5] R. N. Jacobs, J. K. Markunas, C. Nozaki, M. Jaime-Vasquez, P. J. Smith, J. D. Benson, and J. Pellegrino, "Localized dry-etch substrate thinning for dislocation reduction in heteroepitaxial CdTe/Si (211)," J. Vac. Sci. Tech. B 29(3), 03C105 (2011).
[6] V. A. Novikov, D. V. Grigoryev, D. A. Bezrodnyy, and S. A. Dvoretsky, "Distribution of the surface potential of epitaxial HgCdTe," Appl. Phys. Lett. 105(10), 102107 (2014).
[7] N. K. Dhar, P. R. Boyd, M. Martinka, J. H. Dinan, L. A. Almeida, and N. Goldsman, "CdZnTe heteroepitaxy on 3" (112) Si: Interface, surface, and layer characteristics," J. Electron. Mat. 29(6); 748-753 (2000).
[8] R. N. Jacobs, M. J. Vasquez, C. M. Lennon, C. Nozaki, L. A. Almeida, J. Pellegrino, J. Arias, C. Taylor, and B. Wissman, "Dynamic curvature and stress studies for MBE CdTe on Si and GaAs substrates," J. Electron. Mat. 44(9), 3076-3081 (2015).